

Chapter 12

Evaluation from Laboratory to Field Trial of Nanofluids for CaCO₃ Scale Inhibition in Oil Wells



Richard D. Zabala, Carlos A. Franco, Oscar E. Medina, Leidy J. Roldan, C. Candela, José Reyes, German Lucuara, Sergio H. Lopera, Farid B. Cortés, and Camilo A. Franco

12.1 Introduction

Inorganic scale precipitation is a common and recurring problem in the oil and gas industry [1]. Primarily, calcium carbonate (CaCO₃) scales are the most common source of formation damage from precipitation/deposition of mineral scales [1, 2]. The precipitation of inorganic compounds can be developed due to the incompatibility of two fluids [3] or due to the ion concentration that exceeds the solubility under reservoir conditions [4]. Hydrochloric acid (HCl) is frequently used for the remediation of calcium carbonate scales as it offers good short-term performance and low costs [5]. However, these kinds of acid treatments have a short life, and a further decline in production is frequently observed due to scales re-precipitation [6]. Additionally, due to the corrosive nature of HCl, the use of expensive corrosion

R. D. Zabala · C. A. Franco · C. Candela · J. Reyes · G. Lucuara
Departamento de Tecnologías de Producción, Gerencia Técnica, Vicepresidencia Técnica de Desarrollo, Ecopetrol S.A, Bogotá, Colombia
e-mail: richard.zabala@ecopetrol.com.co; carlosal.franco@ecopetrol.com.co; carlos.candela@ecopetrol.com.co; jose.reyesho@ecopetrol.com.co; german.lucuara@ecopetrol.com.co

O. E. Medina · L. J. Roldan · F. B. Cortés (✉) · C. A. Franco (✉)
Química Grupo de Investigación en Fenómenos de Superficie—Michael Polanyi,
Departamento de Procesos y Energía, Facultad de Minas, Universidad Nacional de Colombia – Sede Medellín, Medellín, Colombia
e-mail: oemedinae@unal.edu.co; lejroldanva@unal.edu.co; fbcortes@unal.edu.co; caafrancoar@unal.edu.co

S. H. Lopera
Grupo de Investigación en Yacimientos de Hidrocarburos, Facultad de Minas, Universidad Nacional de Colombia – Sede Medellín, Medellín, Colombia
e-mail: shlopera@unal.edu.co

inhibitors is necessary to protect the injection and pipelines only for a short period [5]. For high-temperature applications, the use of organic acids is preferred because of corrosion problems [1]. The dissolution of calcium carbonate by chelating agents such as ethylenediaminetetraacetic (EDTA) is also well known [7]. These kinds of treatments are less aggressive than acid treatments. However, dissolution rates are slower, and its use in stoichiometric proportions increases costs [8, 9].

The inhibition methods are based on the use of initiation inhibitors, which interact with the nucleation sites of the crystals, limiting their size. Since a little amount of treatment is required, it is an effective way to avoid the deposition of mineral scales [8, 9]. The different inhibitors correspond to one (or more) of the following inhibition mechanisms [10, 11]: (1) crystal distortion, where the inhibitor interferes with the growth of the crystal producing an irregular structure; (2) dispersion, where charges are induced on the surface of the crystal in such a way that the crystals repel each other; (3) chelation, where bonds are formed with certain metal ions forming soluble complexes [12]; and (4) threshold effect, where the inhibitor acts by retarding the precipitation of salts. Phosphonates through the threshold effect prevent nucleation and growth of inorganic scale crystals because they have a high tolerance to Ca^{2+} ions [4, 13]. Additionally, phosphonate-based treatments are stable in a wide range of temperature and pressure at reservoir conditions [14]. These compounds, when used in the formulation of nanofluids, have shown promising results, since, in synergy with nanoparticles (NPs) of different chemical natures, they act on the surface of inorganic scale crystals, affecting their size and morphology [13].

In this sense, nanomaterials and nanofluids are presented as an alternative for the inhibition and/or remediation of formation damage caused by the precipitation of inorganic scales. Due to their small size (1–100 nm) [15, 16], their high surface area [17, 18], their high dispersibility, and their adjustable physicochemical properties, nanomaterials are suitable for injection to reservoir conditions without the risk of blockage and promoting better dispersion throughout the reservoir, including reaching inaccessible places for other types of treatments [19, 20]. The nanoparticles, due to their high reactivity, block the nucleation sites in the inorganic scale crystals, preventing their subsequent growth and precipitation [21, 22]. In this sense, some studies have been focused on the evaluation of different nanoparticles and nanofluids for the CaCO_3 scaling inhibition. Shen et al. [23] found that Ca-diethylenetriamine Penta methylene phosphonic acid (Ca-DTPMP) nanoparticles present good diffusion and retention into the porous media, inhibiting the CaCO_3 precipitation. On the other hand, Zhang et al. [24] found the same results using metal phosphonate-based nanoparticles surrounded by surfactants. Moreover, Haghtalab et al. [25] demonstrated that at 25 °C, the efficiency of Ca-DTPMP nanoparticles for the inhibition and deleting of crystal growth of CaCO_3 increases as the concentration of the inhibitor increases, as well particle size decreases. Other studies include core flooding evaluation at reservoir conditions such as Franco et al. [22], who evaluated Ca-DTIPMP-based nanofluids to inhibit and remediate the CaCO_3 scaling in tight reservoirs. The authors classified the treatment as a threshold inhibitor and founded excellent performance for the inhibition and removal of the formation damage.

Although several researchers have reported on the study of CaCO₃ crystal growth inhibition using nanoparticles as reported above [22, 26, 27], there are few studies focused on the formation damage by inorganic scales under high pH values [26, 27]. This evaluation is important since there are some applications within the chemical enhanced oil recovery (CEOR) such as the injection of alkalis or the alkali-surfactant-polymer (ASP) technique that improve the hydrocarbon sweep efficiency in the reservoir and increase the crude oil recovery factor [28]. However, these applications can produce a collateral effect of raising the pH of the formation water to values that can range between 9 and 11 [19, 28]. This deviation from normal conditions (pH between 6 and 8) cause problems of precipitation of mineral scales due to the incompatibility between formation and injection water [28]. Also, it is worth to mention that, to the best of our knowledge, there is no report about the application of nanofluids for the inhibition from laboratory up to field test in crude oil reservoirs at high pH.

Therefore, the main objective of this work is to evaluate the inhibition efficiency of a homemade nanofluid in the inhibition of the formation damage by precipitation/deposition of CaCO₃ scales at high pH through static and dynamic experiments and its subsequent application in a field test in a Colombian field with previous CaCO₃ scaling due to ASP implementation. The chapter is divided into three sections, including (i) static experiments, where the nanoparticle and nanoparticle/carrier fluid ratio are selected; (ii) dynamic experiments, where the treatment efficiency to inhibit and remediate CaCO₃ scaling damage at reservoir conditions is evaluated; and (iii) field test.

This work, for the first time, reports the execution of a test at field level to inhibit the precipitation of inorganic scales through nanotechnology. In this way, a new landscape is opened, for future applications due to the success of this implementation.

12.2 Materials and Methods

12.2.1 Materials

Commercial TiO₂, CeO₂, and SiO₂ nanoparticles were provided from Sigma Aldrich (St. Louis, MO, USA). The γ -Al₂O₃ nanoparticles were supplied by Petroraza S.A.S. (Sabaneta, Colombia). Sodium hydroxide (NaOH) and MgNO₃·6H₂O (Merck KGaA, Darmstadt, Germany) were used for MgO nanoparticle synthesis. Diethylenetriamine pentamethylene phosphonic acid (DTPMP, 50 wt%) and HCl 37% were provided by Sigma Aldrich (St. Louis, MO, USA). *n*-Hexadecyl-trimethyl ammonium bromide (CTAB) and CaCl₂·2H₂O were purchased for Merck KGaA (Darmstadt, Germany). All these reagents were used for Ca-DTPMP nanoparticle synthesis. For batch experiments, sodium bicarbonate (NaHCO₃, ≥99.7%, Merck KGaA, Darmstadt, Germany) was used. Methanol (99.8% purity) and toluene

(99.8% purity) were employed for porous media cleaning and were obtained from Merck KGaA (Darmstadt, Germany). Sodium chloride (NaCl, 99.5%, Merck KGaA, Darmstadt, Germany) was employed for nanofluid preparation. A commercial EDTA-based treatment “B200” supplied by Petroraza S.A.S. (Sabaneta, Colombia) was employed as carrier fluid (CF) for nanofluid formulation.

Moreover, for the dynamic tests, it has employed a Colombian light crude oil with a 29.9 °API gravity, a viscosity of 40.3 cP at 25 °C, and saturates, aromatics, resins and asphaltenes content of 50.74%, 29.85%, 14.55%, and 4.86% in mass fraction, respectively.

12.2.2 Methods

12.2.2.1 Synthesis of Ca-DTPMP Nanoparticles

The synthesis method of Ca-DTPMP nanoparticles begins by mixing 0.75 M of $\text{CaCl}_2 \cdot 2\text{H}_2\text{O}$ and 3.8% in mass fraction of CTAB in an aqueous solution. The solution is stirred at 300 rpm until a pH of 6.0 is reached. Then, a phosphonate solution of 0.1 M is prepared, and using NaOH the pH is adjusted to 9.0. The phosphonate solution is added dropwise to the $\text{CaCl}_2 \cdot 2\text{H}_2\text{O}$ and stirred for 1 h until a milky white precipitate is observed. The mixture is placed in a water bath for 12 h at 80 °C, filtered, and dried at 100 °C for 12 h. Details of the protocol are reported in a previous study [22].

12.2.2.2 Synthesis of MgO Nanoparticles

MgO nanoparticles were synthesized by the sol-gel technique. The protocol in detail is described in previous work [29]. First, a mixture of 0.2 M of magnesium nitrate and 0.5 M of sodium hydroxide in an aqueous solution was done. The sodium hydroxide was added dropwise to the $\text{MgNO}_3 \cdot 6\text{H}_2\text{O}$ solution until a pH of 12.5 is obtained. The mixture is continuously stirred until a white precipitate is observed. At this point, the mixture is filtered and washed with methanol several times. The remaining solution is centrifugated for 30 min at 4500 rpm and dried at room temperature. Finally, nanoparticles are calcinated at 300 °C for 2 h.

12.2.2.3 Characterization of Nanoparticles

The hydrodynamic size of the nanoparticles was determined through dynamic light scattering (DLS) measurements using a nanoplus-3 (Micromeritics, Norcross, GA, USA). The same equipment was used to obtain the point of zero charge (pH_{pzc}) of the synthesized and commercial nanoparticles in 20 cm³ of deionized water at different pH (from 2 to 10). The surface area (S_{BET}) of the nanoparticles was estimated

following the Brunauer-Emmett-Teller (BET) method by nitrogen adsorption/desorption at $-196\text{ }^{\circ}\text{C}$ in a Gemini VII 2390 from Micromeritics (GA, United States).

12.2.2.4 Nanofluid Preparation

A commercial fluid (CF) named B200 was employed as a carrier fluid for nanoparticle suspension. The properties for the aqueous phase such as density, conductivity, surface tension, and pH were $1.16\text{ g}\cdot\text{mL}^{-1}$, $83.24\text{ }\mu\text{S}\cdot\text{cm}^{-1}$, $27.2\text{ mN}\cdot\text{m}^{-1}$, and 5.52, respectively. CF also was characterized by FTIR to determine chemical composition following protocols described in previous works [16, 22, 30]. The nanofluids were prepared by adding $50\text{ mg}\cdot\text{L}^{-1}$ of nanoparticles to the carrier fluid based on the static results and based on a previous study [22]. The solution is stirred during 2 h at 300 rpm and then sonicated by 1 h to achieve complete distribution of the nanoparticles in the aqueous fluid for being used in the core flooding test. In this order, the nanofluid is composed of Ca-DTPMP nanoparticles and the EDTA-based carrier fluid, without free DTPMP. The stability of the prepared nanofluid was evaluated through zeta potential measurements and ultraviolet-visible technique using a wavelength of 400 nm, following the protocols described in a previous work [16].

12.2.2.5 Batch Experiments for Inhibition of CaCO₃ Scaling

The inorganic scale precipitation/inhibition experiments were performed using synthetic supersaturated calcium carbonate solutions in 100 cm^3 glass vessels at $54.4\text{ }^{\circ}\text{C}$. Following the protocol described in previous work [25], 50 cm^3 of $\text{CaCl}_2\cdot 2\text{H}_2\text{O}$ (0.08 M) were added to the container, then the required amount of nanoparticles was added, and the mixture was subjected to an ultrasound bath for 40 min to guarantee a complete dispersion of the particles in the brine. Subsequently, 50 cm^3 of a NaHCO_3 solution (0.08 M) were added, and the aliquot was taken immediately for the first measurement. The inhibition capacity of CaCO₃ was obtained by measuring Ca^{2+} in solution in the previous mixture. The latter was measured indirectly using an EDTA titration (0.01 M). All experiments were carried out for 140 min. At the end of the titration, the samples were left for 8 h at $54.4\text{ }^{\circ}\text{C}$, and a final aliquot was taken. pH was adjusted to 10 for scaling evaluation and was monitored during the test. Equation 12.1 was used to calculate the inhibition efficiency (%Inh) of nanofluid:

$$\% \text{Inh} = \frac{C_a - C_b}{C_c - C_b} \times 100 \quad (12.1)$$

where C_a , C_b , and C_c are the concentration of Ca^{2+} in the treated sample after precipitation, in the blank after precipitation (system without nanoparticles), and in blank before precipitation, respectively. Additionally, the size of the CaCO₃ crystals formed in the presence and absence of the nanofluid was evaluated by DLS. Batch experiments were carried out for different nanoparticles. Then, the nanoparticle

with the best yield was selected for nanofluid formulation using the commercial carrier fluid.

12.2.2.6 Core Flooding Tests

To evaluate the efficiency of the nanofluid for inhibiting and remediating CaCO_3 scaling at high pH, core flooding experiments were developed. A Colombian sandstone core of a hydrocarbon was employed, and its petrophysical properties are shown in Table 12.1. The sandstone core is composed of 99.0% in a mass fraction of quartz and 1.0% in a mass fraction of a mixture of clays, including kaolinite, chlorite, and illite. The evaluation of the nanofluid in the inhibition and remediation of the formation damage caused by mineral scales was carried out mainly in three stages: (i) evaluation of the base permeabilities, (ii) damage inhibition, and (iii) damage remediation.

Initially, 10 pore volumes (PV) of reservoir brine composed by 2.0% in mass fraction of KCl were injected at a fixed flow rate of $0.3 \text{ cm}^3 \cdot \text{min}^{-1}$ for measuring the absolute permeability of the system. Then, 10 PV of oil are injected, and the effective oil permeability is measured at residual water saturation (S_{wr}). Subsequently, 10 PV of the reservoir brine is injected again, and the effective permeability to water at residual oil (S_{or}) is determined. For the inhibition experiment, 3 PV of the Ca-DTPMP-based nanofluid are injected and left for a soaking time of 8 h. Next, the damage is generated by the injection of incompatible brines. Oil and brine are injected again to obtain K_o , K_w , K_{ro} , and K_{rw} . Then, if the inhibition is effective, the durability of the treatment is evaluated by injecting 10 PV of two problematic brines, composed of 0.08 M of NaHCO_3 solution (B1) and 0.08 M of $\text{CaCl}_2 \cdot 2\text{H}_2\text{O}$ solution (B2) two more times and evaluating K_{ro} , K_{rw} , and K_w with the injection of 10 PV of crude oil and 10 PV of KCl-based brine. The experimental conditions were kept constant during each perdurability test.

In the next stage, remediation damage efficiency is evaluated. At this point, the damage is generated from the injection of 10 PV of B1 and B2 brines. The mixture of these incompatible brines provides the CaCO_3 scale formation. Subsequently, the reduction in K_{ro} , K_{rw} , and K_w is quantified by saturating the medium with crude oil and 2% in mass fraction of KCl synthetic brine. At this point, the injection of 3 PV of the nanofluid is performed. The system is then soaked for 8 h. The effect will be evaluated by changing the permeabilities of the system by injecting oil and synthetic brine.

Table 12.1 Properties of porous media employed for the core flooding experiments

Property	Value
Length	7.05 cm
Diameter	3.80 cm
Porosity	16%

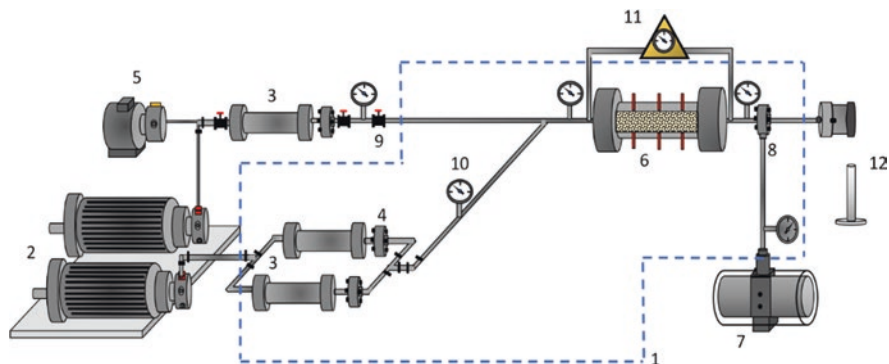


Fig. 12.1 Experimental setup for the displacement test. Legend: (1) oven (framed in dotted blue line), (2) the positive displacement pump, (3) displacement cylinders, (4) filters, (5) electric hydraulic pump, (6) the core holder, (7) the pressure multiplier, (8) the backpressure system, (9) valve, (10) manometer, (11) pressure transducer, and (12) the graduated cylinder

After the removal and quantification stage of the damage remediation, the encrusting brines B1 and B2 are injected again to try to induce damage by calcium carbonate scales to evaluate the effectiveness of a single treatment injection for removing the mineral scale formation damage. In this sense, the inorganic scale precipitation is induced, and the pressure differential is recorded during the injection of each one of the fluids, reservoir brine, and crude oil.

The core flooding tests were done at 54.4 °C (130 °F) and confining and pore pressures of 1800 and 300 psi, respectively. Figure 12.1 shows a representative diagram of the experimental setup used, consisting of three displacement cylinders (Max Servicios S.A.S., Colombia) that contain the synthetic brines, nanofluid and crude oil, positive displacement pumps (DB Robinson Group, Edmonton, AB, Canada), an electric hydraulic pump (Enercap, Actuant Corporation, WI, USA), a core holder along with the sand pack, manometers (Rosemount, Emerson, MO, USA), and valves (Swagelok, OH, USA).

12.3 Results

12.3.1 Carrier Fluid and Nanoparticles Characterization

Figure 12.2 shows the FTIR spectra obtained. Results show a predominant band between 3450 and 3500 cm⁻¹ assigned to N–H stretching or free –OH groups. The IR bands located between 769 and 1100 cm⁻¹ are related to N–H stretching or overlapping to C–C groups. Also, the band at 1641 cm⁻¹ is due to the stretching vibrations of C=O bonds. Hence, the results confirm that the CF is EDTA based.

Table 12.2 shows the mean hydrodynamic diameter of the nanoparticles. For commercial fumed silica (SiO₂) nanoparticles, aluminum oxide (Al₂O₃), and ceria

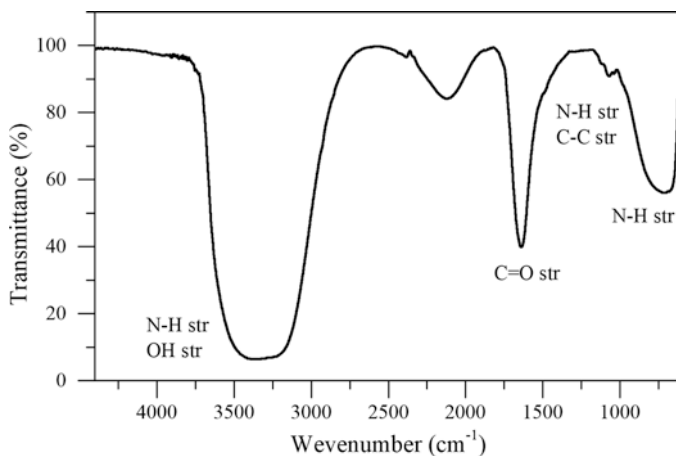


Fig. 12.2 FTIR spectra of carrier fluid

Table 12.2 Mean particle size (d_{50}), BET surface area (S_{BET}), and point of zero charge (pH_{pzc}) of nanoparticles

Nanoparticle	d_{50} (nm)	S_{BET}	pH_{pzc}
Ca-DTPMP	66.0	46.0	9.0
SiO ₂	11.0	382.0	3.0
Al ₂ O ₃	35.0	277.0	9.0
CeO ₂	22.0	64.0	7.5
MgO	80.0	230.0	11.0

(CeO₂), a hydrodynamic diameter median of 11, 35 and 22 nm, respectively, was obtained. In the case of the synthesized magnesium oxides (MgO) and Ca-DTPMP nanoparticles, the mean hydrodynamic diameters are 80 and 66 nm, respectively. Besides, the surface area increases in the order Ca-DTPMP < CeO₂ < MgO < Al₂O₃ < SiO₂. It is important to mention that the nanoparticles are nonporous. These results are according to the report in the literature [15, 22, 29]. As for the pH_{pzc} values, above $pH = 7$, Al₂O₃, CeO₂, MgO, and Ca-DTPMP nanoparticles acquire a positive surface charge, and SiO₂-nanoparticles acquire a negative charge [31]. In the presence of the carrier fluid, for the pH of scaling evaluation close to 10, nanoparticles Ca-DTPMP, Al₂O₃, CeO₂, MgO, and SiO₂ acquire a Zeta potential value around -60 mV, -30 mV, -5 mV, -8 mV, and 14 mV, respectively. Therefore, it is expected that Ca-DTPMP nanoparticles are more dispersed in the carrier fluid than the other systems, leading to high stability during the injection process.

12.3.2 Selection of Nanoparticle by Batch Experiments for CaCO₃ Scaling Inhibition

Table 12.3 summarizes the inhibition efficiency for CaCO₃ precipitation of the different nanoparticles after 2 and 8 h. As a first instance, the efficiencies are greater during the first 2 h, and a considerable decrease is observed after 8 h. This behavior can be explained since nanoparticles get attached to the active growth sites of calcium carbonate, changing the pattern of growth and slowing down the crystal formation process. After 8 h, a decrease in the efficiency of each nanoparticle is observed. These substantial differences can be mainly associated with the fact that during the first 2 h of the experiment, the growth of inorganic scale crystals occurs. At this point, the nanoparticles, through different interactions, are adsorbed on the crystals, changing the growth pattern and slowing down the crystal formation process [22, 23]. However, a balance in crystal growth has not yet been achieved; hence, there is desorption of the calcium carbonate crystal inhibitor, allowing it to grow easier. This implies that an adsorption/desorption equilibrium occurs for a higher time. Probably, for 8 h, the system gets the equilibrium, and it was corroborated by Ca²⁺ ion concentration, which remains constant after 140 min.

As for the nanoparticle chemical nature effect, the inhibition efficiency increases in the order MgO < CeO₂ < Al₂O₃ < SiO₂ < Ca-DTPMP for both times. In general, the presence of nanoparticulated materials inhibits the precipitation of Ca²⁺ ions. Following the theory of the electric double layer, positively charged ions on the surface of the nanoparticle attract the most negatively charged (CO₃²⁻), which will form a layer around the surface. This agrees with our previous results [22]. These ions can interact with Mg²⁺, Ce³⁺, and Al³⁺ ions present in MgO, CeO₂, and Al₂O₃ nanoparticle surface, respectively. This, in turn, CO₃²⁻ will attract the most positively charged ions (Ca²⁺), formatting an outer layer rich in cations around the carbonate ion layer. The presence of dipole moments in the solution could promote multiple layer formation within the double layer and thus aid in arranging the ions in a favorable pattern for crystallization [32].

Moreover, due to the threshold inhibitor mechanism, the Ca-DTPMP nanoparticles control and prevent the growth of CaCO₃ scales to a higher degree than the rest

Table 12.3 Inhibition efficiencies for CaCO₃ precipitation at 54.4 °C using 50 mg•L⁻¹ of different nanoparticles

Nanoparticle	Inhibition efficiency	
	2 h	8 h
Ca-DTPMP	63.0	25.0
SiO ₂	57.1	20.2
Al ₂ O ₃	55.0	18.3
CeO ₂	54.3	18.2
MgO	48.3	17.4

of nanoparticles, mainly by the interactions with the functional groups P–OH and P–O–Ca on the crystal structure. The nano-Ca-DTPMP allows retaining the Ca^{2+} concentrations in the bulk solutions [22]. These results are in agreement with the report by [22], where it was demonstrated that the CaCO_3 crystals obtained by using of Ca-DTPMP nanoparticles as an inhibitor present softer textures, amorphous structures, less amount of adherents, and, therefore, less restriction to be transported through the porous media and production lines.

12.3.3 Nanofluid Selection by Batch Experiments for Inhibition of CaCO_3 Scaling

In this section, the Ca-DTPMP/CF ratio was evaluated by varying the concentration of the nanoparticles in the carrier fluid. The concentrations evaluated were 50, 250, 1000, and 2000 $\text{mg}\cdot\text{L}^{-1}$, obtaining Ca-DTPMP/CF ratio of 10, 50, 200, and 400, respectively.

Both the inhibitor (Ca-DTPMP nanoparticles-aqueous solution) and the carrier fluid were evaluated in the absence of nanoparticles, at a fixed Ca-DTPMP/CF ratio. Efficiencies less than 15% were obtained at 2 h, due to the chelating effect of EDTA. As CF is composed by EDTA, good performance can be obtained under a correct stoichiometric ratio, where the scaling process can be inhibited by chelating/sequestering the scaling cation. Table 12.4 shows the efficiencies of calcium carbonate precipitation inhibition, obtained with the Ca-DTPMP-based nanofluid, for different Ca-DTPMP/CF ratios and the effect of CF without nanofluids. In this test, the mixture of the calcium chloride and sodium bicarbonate brines was carried out to promote the calcium carbonate precipitate, and the addition of the nanofluid was done to inhibit this precipitation. The efficiencies were determined through the concentration of calcium in the solution for the periods of 2 and 8 h, based on a blank sample, which consisted of the brine mixture, without adding treatment for inhibition. From Table 12.4 it is observed that the carrier fluid has the lowest inhibition efficiency. However, the inhibition efficiency achieved is due to the chemical nature of the phosphonate-based fluid. These chemical inhibitors require a low number of

Table 12.4 Inhibition efficiencies for CaCO_3 precipitation at 54.4 °C at different Ca-DTPMP/CF ratios

Ca-DTPMP/CF ratio	Inhibition efficiency	
	2 h	8 h
CF without nanoparticles	35.0	13.0
10	100.0	87.0
50	87.0	80.0
200	78.0	48.0
400	60.0	38.0

growth inhibitory molecules to prevent the growth of mineral scales, blocking nucleation, through interaction with crystal nucleation sites, and avoiding contact between ions. Phosphonates act under a chelation effect either by inhibition of nucleation or retardation of crystal growth. Besides, the inhibition efficiencies obtained with nanofluids are higher than those obtained by evaluating only nanoparticles. The interaction of the nanoparticles with the synthesis fluid allows having a system where the nanoparticles are adsorbed on the active growth sites of calcium carbonate, delaying their growth [13, 23]. The carrier fluid helps to dissolve the precipitate because the action of the nanoparticles on the crystal makes it softer, more unstable, and less adherent, so that the amount of precipitate generated decreases considerably, as well as the difference between the efficiencies of the two periods evaluated, achieving a more efficient treatment in the inhibition of CaCO₃ precipitation due to its chemical nature. Moreover, the acidic character of the CF may lead to the dissolution of CaCO₃ crystals, and hence higher inhibition efficiency is obtained.

In addition, according to the zeta potential at scaling evaluation conditions, low agglomeration of the Ca-DTPMP nanoparticles is achieved due to its high dispersion, leading to higher coverage of the CaCO₃ crystals. Furthermore, the analysis ensured the low agglomeration of nanoparticles since no significant change in light absorption was detected.

The highest inhibition efficiency at 2 and 8 h was obtained with the nanofluid prepared with a Ca-DTPMP/CF ratio of 10. This is due to the negative charge that the nanoparticles acquire in the CF for the working pH, added to the colloidal stability of the system for low Ca-DTPMP/CF reactions. For a ratio of 10, the nanoparticles are more dispersed in the nanofluid, with a zeta potential value of -22 . Less agglomeration allows a greater coverage of the CaCO₃ crystals and therefore a greater inhibition efficiency. The systems with ratios of 200 and 500, despite having a higher content of the scale inhibitor, their Z potential values for the working pH, are around -10 . Despite being negatively charged, their tendency to agglomerate is much greater, and therefore their efficiency decreases. It can be concluded that nanoparticles have a synergistic effect with the carrier fluid, improving or adding inhibition mechanisms according to their stability. The formation of soluble complexes was not observed, as it is common in the presence of ferrous oxides [33, 34].

12.3.4 Core Flooding Test

12.3.4.1 Inhibition of CaCO₃ Scaling

Figure 12.3a, b shows the relative permeability and oil recovery curves for nanoparticles and carrier fluid, independently evaluated. According to the results, the injection of the nanoparticles and the carrier fluid generate a reduction in the residual oil saturation, obtaining better results for the Ca-DTPMP nanoparticles than for the carrier fluid. In addition, the slopes of both curves change slightly compared to the

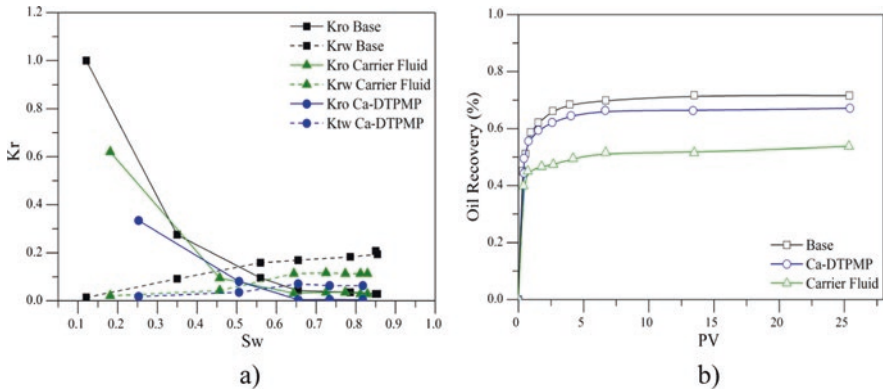


Fig. 12.3 (a) Relative permeability curves and (b) oil recovery curves for the inhibition of CaCO_3 precipitation using $50 \text{ mg}\cdot\text{L}^{-1}$ of Ca-DTPMP and carrier fluid. Temperature at $54.4 \text{ }^\circ\text{C}$ ($130 \text{ }^\circ\text{F}$) and confining and pore pressures of 1800 and 300 psi

Table 12.5 Values of oil and water effective permeabilities for the inhibition of CaCO_3 precipitation using $50 \text{ mg}\cdot\text{L}^{-1}$ of Ca-DTPMP-based nanofluid. Temperature at $54.4 \text{ }^\circ\text{C}$ ($130 \text{ }^\circ\text{F}$) and confining and pore pressures of 1800 psi and 300 psi

Phase	K_w (mD)	K_o (mD)
Base	25.0	43.0
<i>Perdurability 1</i>	24.0	42.0
<i>Perdurability 2</i>	24.0	41.5
<i>Perdurability 3</i>	19.0	39.0

baseline, keeping the K_{ro} slope greater than K_{rw} . Similarly, the curves move to the right, to a greater degree for nanoparticles, showing their ability to keep the system highly wettable to water. On the other hand, panel b of the same Fig. 12.3b shows that the amount of recovered oil is greater for the Ca-DTPMP nanoparticles than for the carrier fluid. However, both show high efficiencies due to the chelating effect of the CF and the ability of the nanoparticles to prevent the growth of CaCO_3 crystals.

Besides, the obtained permeability values are presented after the injection of the nanofluid and after the induction of damage by injecting 10 pore volumes of incompatible brines. Also, the durability of the treatment was evaluated. It should be noted that the injected nanofluid had a soaking time of 8 h. Then, CaCO_3 scaling damage was produced three times to evaluate the perdurability of the treatment. Each stage was referred as *perdurability 1 (P1)*, *perdurability 2 (P2)*, and *perdurability 3 (P3)*. Table 12.5 shows the behavior of the oil and water effective permeabilities in the damage inhibition phase. For water, during the three injections of B1 and B2, the permeability slightly falls from 25 mD to 24 mD, 24 mD, and 19 mD, respectively. For the *perdurability 3* stage, the system decreases its effectiveness at a low extent. The results indicate that the nanofluid has a high ability to maintain effective water

permeability close to its initial even though several pore volumes were injected. Analogous to the effective water permeability data, the oil permeability showed similar behavior, with reductions from 43 mD to 42, 41, and 39 mD for the first, second, and third evaluation of the permeability, respectively. However, in the third evaluation, the K_o only decreased by 10%, showing better results than the K_w reduction. It is important to mention that the measurements for the base system were taken before the flooding of the incompatible brines.

Figure 12.4a shows the base relative permeability curves and the respective curves for the three durability evaluations. The base curve indicates a water-wet porous medium due to the high value of K_{ro} at residual water saturation, a slightly higher slope of the K_{ro} curve compared to that of K_{rw} , and finally, a high value of the residual saturation of water concerning that of oil. In each durability evaluation phase, both the water and oil relative permeability curves are reduced. Analogous to the reduction of the effective permeability curves, the system does not undergo substantial changes in the first two evaluations of durability. In the third evaluation, the K_{ro} and K_{rw} fall sharply, and the residual saturations increase. In the case of *perdurability 2*, it can be noted that the curves shift to the right, indicating that the system

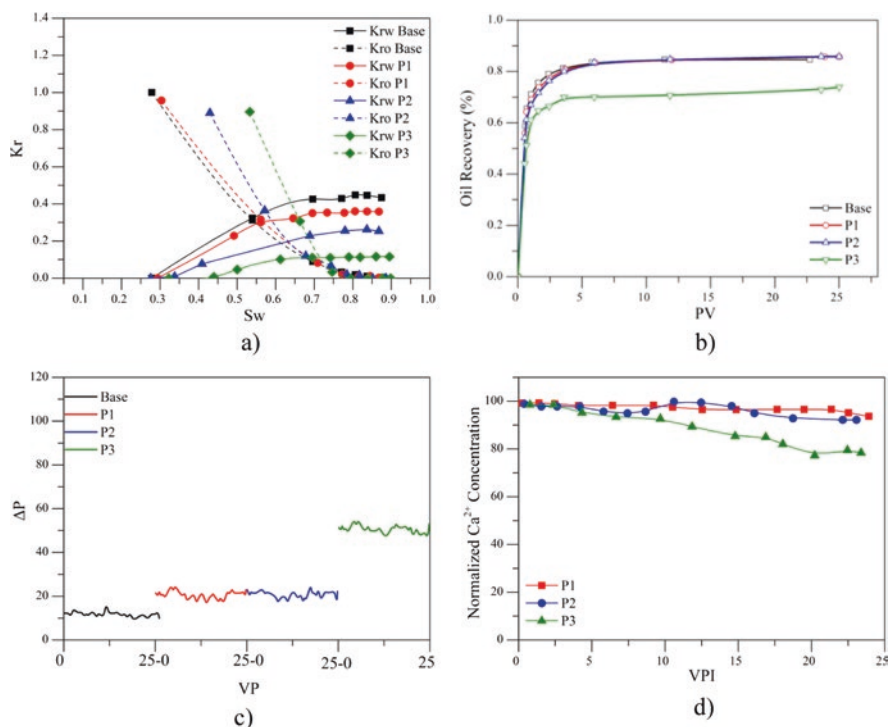


Fig. 12.4 (a) Relative permeability curves, (b) oil recovery curves, (c) pressure drop and (d) normalized Ca²⁺ concentration profiles in effluents for the inhibition of CaCO₃ precipitation using 50 mg•L⁻¹ of Ca-DTPMP-based nanofluid. Temperature at 54.4 °C (130 °F) and confining and pore pressures of 1800 and 300 psi

is changing to a strong water-wet condition. On the other hand, the residual oil saturation was reduced. Also, the mobility to water is reduced. In the case of *perdurability* 3, there is no significant decrease in residual oil saturation. However, there is a higher irreducible water saturation compared to the previous cases, implying an increase in water wettability. There is also a decrease in the mobility of water concerning the base. Besides, the oil recovery curves and the behavior of the nanofluid as an inhibitor are presented in Fig. 12.4b. The first two *perdurability* evaluations do not undergo major changes, while for the third durability evaluation, the system does not inhibit efficiently, and scale deposition occurs, leading to an oil recovery reduction of 9%.

Figure 12.4c shows the pressure drop profiles for each stage. For the base curve, the pressure drop stabilizes near 10 psi. Then, during the inhibition processes, the pressure drops increase by 55%, and the value is maintained until the *perdurability* 2 stage. Finally, during *perdurability* 3, pressure drop increases to approximately 60 psi, which is in accordance with the oil and water permeabilities. On the other hand, Fig. 12.4d shows the profiles for the Ca^{2+} concentration in the recovered effluents that were analyzed following the same procedure of batch experiments. Results show that during each inhibition stage, there is a correct performance of the nanofluids, avoiding the scaling of inorganic scales in porous media. Finally, the pH was monitored in the collected water effluents, obtaining insignificant variations.

12.3.4.2 Remediation of CaCO_3 Scaling

Remediation of mineral scaling formation damage was evaluated in two main stages. Initially, the damage was caused by the deposition of inorganic calcium carbonate scales by the injection B1 and B2 in the porous medium. Then, the effectiveness of Ca-DTPMP nanoparticles, CF, and nanofluid was analyzed. Figure 12.5a

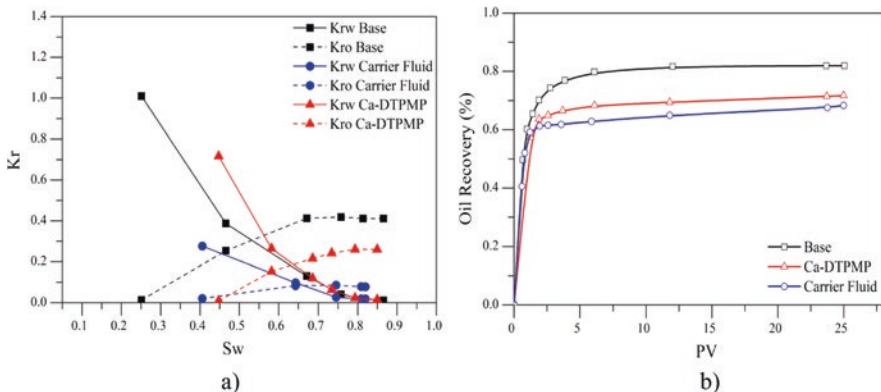


Fig. 12.5 (a) Relative permeability curves and (b) oil recovery curves for the remediation of CaCO_3 precipitation using $50 \text{ mg}\cdot\text{L}^{-1}$ of Ca-DTPMP and carrier fluid. Temperature at $54.4 \text{ }^\circ\text{C}$ ($130 \text{ }^\circ\text{F}$) and confining and pore pressures of 1800 psi and 300 psi

shows relative permeability curves for Ca-DTPMP nanoparticles and CF. In the first instance, it is observed that both the CF and the nanoparticles dissipate the S_{or} after the remediation of the formation damage. In addition, the system in both cases maintains its preference to be wet by the water, reflected in the displacement of the K_r to the right. As for the recovery of the OOIP, shown in Fig. 12.5b, this was greater for the nanoparticles than for the CF. Like the inhibition process, both systems present good results when evaluated individually.

For nanofluid evaluation, the changes in the permeability of both the oil and water phase are summarized in Table 12.6. From the results, it is observed that by depositing inorganic scales, formation damage of 57% is generated according to the reduction of the K_w values. When injecting the nanofluid for permeability restoration, a K_w above the base water permeability was obtained. This suggests that the treatment removes the deposited inorganic scales and improves the flow conditions of the system.

Regarding the oil effective permeabilities (K_o), it is observed that after the treatment injection, there is an increase of 13% compared to the base permeability. Hence, it can be said that the treatment not only removes mineral scaling formation damage but also favors the flow conditions of water and oil in the porous medium.

Figure 12.6 shows the relative permeability curves and the oil recovery curves for the systems after damage caused by inorganic scales deposition and after the damage removal with the nanofluid. From panel a of Fig. 12.6, it can be identified that when damage is generated, the residual saturation of both the water and oil increase; therefore, the mobility of both phases is strongly affected. After the treatment injection, the medium becomes more wetttable to the water and recovers the mobility of oil and water phases; however, it should be noted that the mobility of the water remains slightly below to the base, while that of the oil tends to overcome the basic mobility conditions.

Figure 12.6b shows the results of the oil recovery curves during the damage removal stage. Once the damage caused by scale deposition is generated, only a recovery of 37% of the original oil in place is obtained. After treatment injection, a recovery 3% higher to the base scenario is achieved. It is validated again that the treatment not only removes the damage but also improves the rock and fluid conditions, allowing recovery values to be reached above the base conditions (scenario without damage).

Table 12.6 Values of oil and water effective permeabilities for the remediation of CaCO₃ precipitation using 50 mg•L⁻¹ of Ca-DTPMP-based nanofluid. Temperature at 54.4 °C (130 °F) and confining and pore pressures of 1800 psi and 300 psi

Phase	K_w (mD)	K_o (mD)
Base	28.0	45.0
Damage	16.0	25.0
Nanofluid injection	29.0	61.0

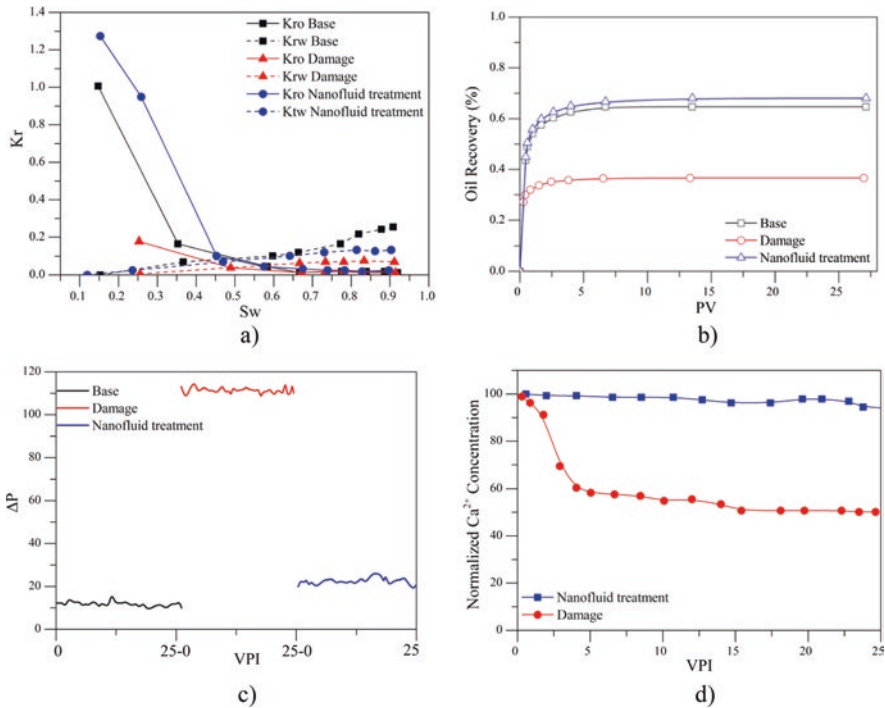


Fig. 12.6 (a) Relative permeability curves, (b) oil recovery curves, (c) pressure drop, and (d) normalized Ca²⁺ concentration profiles in effluents for the remediation of CaCO₃ precipitation using 50 mg•L⁻¹ of Ca-DTPMP-based nanofluid. Temperature at 54.4 °C (130 °F) and confining and pore pressures of 1800 and 300 psi

On the other hand, the pressure drop profiles are presented in Fig. 12.6c. For the baseline, the pressure drop is adjusted to 11 psi. The fall is associated with the movement of fluids during oil recovery. After damage induction, the values increase to 116 psi, and, finally, after the injection of nanofluids, the value stabilizes at around 20 psi. Finally, the effluents recovered in both stages were analyzed by Ca²⁺ concentration and are showed in Fig. 12.6d. The results indicate that after the removal of formation damage, a negligible concentration of Ca²⁺ ions is observed in the recovered effluents, which corroborates the high efficiency of nanofluids to remedy damage due to mineral scaling. Finally, the pH was monitored in the collected water effluents, in which no variation was observed in its value, that is, the high pH was maintained during the experiment.

12.3.5 Field Trial

Based on the static and dynamic results on the evaluation of the inhibition of the precipitation of inorganic scales, a pilot test was designed in an oil field in Southern Colombia. The brine was composed by 13,500 mg•L⁻¹ of Na⁺, 185 mg•L⁻¹ of K⁺, 394 mg•L⁻¹ of Mg⁺⁺, 7600 mg•L⁻¹ of Ca⁺⁺, 390 mg•L⁻¹ of Sr⁺⁺, 31 mg•L⁻¹ of Fe⁺⁺, 35,454 mg•L⁻¹ of Cl⁻, 80 mg•L⁻¹ of SO₄⁻, and 128 mg•L⁻¹ of HCO₃⁻, indicating that the experimental conditions evaluated represented a more drastic scenario for the CaCO₃ scaling.

The chosen well was completely closed, and its production was zero barrels per day due to the conditions obtained after the alkali-surfactant polymer (ASP) flooding process to which it was exposed during years. The results obtained with the EOR process were not successful, leading to high pH values in the reservoir water, which favored the precipitation of the calcium carbonate in the near-wellbore area. The CO₂ content, in this case, was negligible, which indicates that the main damage mechanism is related to brines incompatibility and high pH values. In this sense, the nanofluid with the best results for the remediation and inhibition of the formation damage by inorganic scale was injected in the field trial. As the selected well had an electric submersible pump (ESP) for artificial lift, the nanofluid was injected through the annular and left to soak during 12 h. Figure 12.7 shows the results of the pilot test carried out in a field in Southern Colombia. The porosity of this field is between 15% and 20% with an average permeability of 2500 mD.

The blue shaded box coincides with an ASP stimulation treatment carried out between January 2014 and January 2015 that resulted in a complete cessation of production attributed to formation damage due to precipitation/deposition of calcite

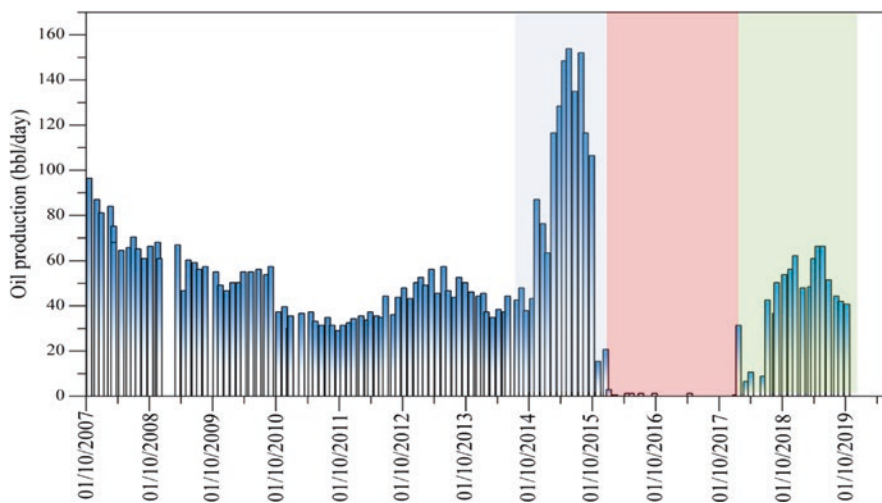


Fig. 12.7 Pilot test: Evaluation of the efficiency of the nanofluid in the removal and inhibition of damage by precipitation/deposition of mineral scales

scales for the alteration of the pH of the formation water, which leads to formation damage for inorganic scales.

In January 2017, it started with the injection of the nanofluid (green box). The implementation was successful showing an increase in oil production of 66 barrels per day during the first year of production after a total cessation of approximately 1 year. After 24 months of monitoring, oil production remains above the baseline. This result showed the ability of the nanofluid for remediating and inhibiting calcium carbonate precipitation/deposition formation damage under high pH conditions. It is worth mentioning that this phenomenological approach is based on fluid-fluid and fluid-surface interactions that lead to the successful formulation of a nanotechnology-based chemical treatment that can remediate and inhibit this formation damage.

The nanoparticle concentration was monitored after the well is open for production, as shown in Fig. 12.8. It is observed that, after the job, concentrations of nanoparticles lower than $20 \text{ mg}\cdot\text{L}^{-1}$ are obtained, indicating a high interaction with the porous medium and leading to high perdurability of the treatment. It is worth mentioning that, as an additional benefit of the treatment, the lifting costs were reduced. Before nanofluid, the ESP constantly failed due to the CaCO_3 scaling and the well-needed intervention every 40 days. After the nanofluid injection, the production was constant for more than 1 year without the need for well intervention.

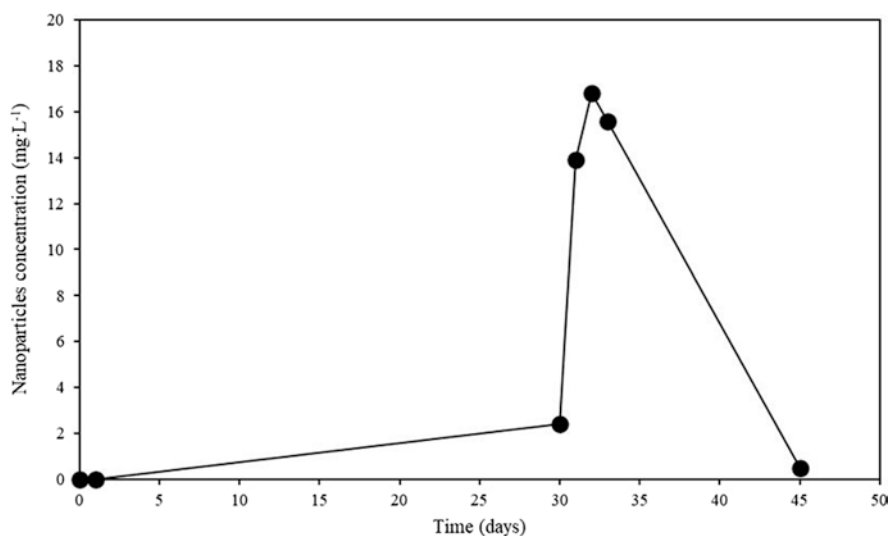


Fig. 12.8 Nanoparticles tracking after the stimulation process

12.4 Conclusion

Static tests at high pH show a 100% inhibition percentage of the damage caused by inorganic scales in the presence of the Ca-DTPMP-based nanofluid. The nanofluid evaluated can be identified as a double effect inhibitor that acts on the calcite crystals limiting their growth. The synergistic effect between the nanoparticles and the transport fluid is evident, which shows an excellent performance both in the elimination and in the inhibition of the formation damage of mineral scales at high pH and reservoir conditions. Dynamic inhibition tests also show the excellent durability of the treatment. Finally, the implementation of the technology in the field was successful showing an increase in oil production of 66 barrels per day during the first year of production. After 24 months of monitoring, oil production remains above the baseline. Due to these field results, the technology was implemented in other wells in the field and expanded to other fields. The economy of the project is greatly improved because in the stimulation/inhibition work strategy, it was reduced from 2 to 1 stage because the wells are stimulated and inhibited in a single program and not in two stages, as is normally done.

Acknowledgments The authors would like to acknowledge to ECOPETROL S.A and Universidad Nacional de Colombia for their logistical, technical, and financial support. At the same time, the authors also acknowledge Grupo de Investigación en Fenómenos de Superficie-Michael Polanyi.

References

1. P. Smith, C. Clement Jr, A.M. Rojas, Combined scale removal and scale inhibition treatments, in *International Symposium on Oilfield Scale* (2000)
2. T. Østvold, P. Randhol, Kinetics of CaCO₃ scale formation. The influence of temperature, supersaturation and ionic composition, in *International Symposium on Oilfield Scale* (2001)
3. A. Khormali, D.G. Petrakov, Laboratory investigation of a new scale inhibitor for preventing calcium carbonate precipitation in oil reservoirs and production equipment. *Pet. Sci.* **13**, 320–327 (2016)
4. A.B. Merdhah, A. Yassin, Formation damage due to scale formation in porous media resulting water injection. *System* **14**, 15 (2008)
5. F.F. Chang, H.A. Nasr-El-Din, T. Lindvig, X. Qui, Matrix acidizing of carbonate reservoirs using organic acids and mixture of HCl and organic acids, in *SPE Annual Technical Conference and Exhibition* (2008)
6. C. Wang, S.-P. Li, T.-D. Li, Calcium carbonate inhibition by a phosphonate-terminated poly (maleic-co-sulfonate) polymeric inhibitor. *Desalination* **249**, 1–4 (2009)
7. A. Tariq, N. Jun Hong, H. Nasr-El-Din, Chelating agents in productivity enhancement: A review, in *SPE Oklahoma City Oil and Gas Symposium* (2017)
8. K. Malave Tomala, A.E. Larrea Idiarte, Estudio de problemas de incrustaciones y evaluación de químicos anti-incrustantes en núcleos seleccionados para diseños de tratamientos tipo “squeeze” a las areniscas uyt del campo shushufindi, Thesis, Escuela Superior Politécnica del Litoral (ESPOL), Guayaquil, Ecuador (2009)
9. M.S. Kamal, I. Hussein, M. Mahmoud, A.S. Sultan, M.A. Saad, Oilfield scale formation and chemical removal: A review. *J. Pet. Sci. Eng.* **171**, 127–139 (2018)

10. P.G. Koutsoukos, P. Klepetsanis, N. Spanos, D. Kanellopoulou, Calcium carbonate crystal growth and dissolution inhibitors, in *CORROSION 2007* (2007)
11. K. Sawada, The mechanisms of crystallization and transformation of calcium carbonates. *Pure Appl. Chem.* **69**, 921–928 (1997)
12. M. Finšgar, J. Jackson, Application of corrosion inhibitors for steels in acidic media for the oil and gas industry: A review. *Corros. Sci.* **86**, 17–41 (2014)
13. B. Zhang, L. Zhang, F. Li, W. Hu, P.M. Hannam, Testing the formation of Ca–phosphonate precipitates and evaluating the anionic polymers as Ca–phosphonate precipitates and CaCO₃ scale inhibitor in simulated cooling water. *Corros. Sci.* **52**, 3883–3890 (2010)
14. F.H. Browning, H.S. Fogler, Effect of precipitating conditions on the formation of calcium – HEDP precipitates. *Langmuir* **12**, 5231–5238 (1996)
15. O.E. Medina, J. Gallego, D. Arias-Madrid, F.B. Cortés, C.A. Franco, Optimization of the load of transition metal oxides (Fe₂O₃, Co₃O₄, NiO and/or PdO) onto CeO₂ nanoparticles in catalytic steam decomposition of n-C₇ asphaltenes at low temperatures. *Nano* **9**, 401 (2019)
16. O.E. Medina, Y. Hurtado, C. Caro-Velez, F.B. Cortés, M. Riazi, S.H. Lopera, et al., Improvement of steam injection processes through nanotechnology: An approach through in situ upgrading and foam injection. *Energies* **12**, 4633 (2019)
17. O.E. Medina, C. Olmos, S.H. Lopera, F.B. Cortés, C.A. Franco, Nanotechnology applied to thermal enhanced oil recovery processes: A review. *Energies* **12**, 4671 (2019)
18. O.E. Medina, J. Gallego, L.G. Restrepo, F.B. Cortés, C.A. Franco, Influence of the Ce⁴⁺/Ce³⁺ redox-couple on the cyclic regeneration for adsorptive and catalytic performance of NiO–PdO/CeO₂±δ nanoparticles for n-C₇ asphaltene steam gasification. *Nano* **9**, 734 (2019)
19. S.B. Márquez, F.B. Cortés, F.C. Marín, Desarrollo de Nanopartículas Basadas en Sílice para la Inhibición de la Precipitación/Deposición de Asfaltenos. MSc Investigación, Ingeniería de Petróleos, Universidad Nacional de Medellín (2015)
20. O.E. Medina, C. Caro-Vélez, J. Gallego, F.B. Cortés, S.H. Lopera, C.A. Franco, Upgrading of extra-heavy crude oils by dispersed injection of NiO–PdO/CeO₂±δ nanocatalyst-based nanofluids in the steam. *Nano* **9**, 1755 (2019)
21. C.A. Franco, N.N. Nassar, M.A. Ruiz, P. Pereira-Almao, F.B. Cortés, Nanoparticles for inhibition of asphaltenes damage: Adsorption study and displacement test on porous media. *Energy Fuel* **27**, 2899–2907 (2013)
22. M. Franco-Aguirre, R.D. Zabala, S.H. Lopera, C.A. Franco, F.B. Cortés, Ca-DTPMP nanoparticles-based nanofluids for the inhibition and remediation of formation damage due to CaCO₃ scaling in tight gas-condensate reservoirs. *J. Pet. Sci. Eng.* **169**, 636–645 (2018)
23. D. Shen, P. Zhang, A.T. Kan, G. Fu, H.A. Alsaïari, M.B. Tomson, Control placement of scale inhibitors in the formation with stable Ca-DTPMP nanoparticle suspension and its transport in porous medium, in *SPE International Oilfield Scale Conference* (2008)
24. P. Zhang, D. Shen, C. Fan, A. Kan, M. Tomson, Surfactant-assisted synthesis of metal-phosphonate inhibitor nanoparticles and transport in porous media. *SPE J.* **15**, 610–617 (2010)
25. A. Haghtalab, Z. Kiaei, Evaluation of the effective parameters in synthesis of the nano-structured scaling inhibitors applicable in oil fields with sea water injection process. *J. Nanopart. Res.* **14**, 1210 (2012)
26. J. Guo, S.J. Severtson, Inhibition of calcium carbonate nucleation with aminophosphonates at high temperature, pH and ionic strength. *Ind. Eng. Chem. Res.* **43**, 5411–5417 (2004)
27. J. Guo, S.J. Severtson, Application of classical nucleation theory to characterize the influence of carboxylate-containing additives on CaCO₃ nucleation at high temperature, pH, and ionic strength. *Ind. Eng. Chem. Res.* **42**, 3480–3486 (2003)
28. A.A. Olajire, Review of ASP EOR (alkaline surfactant polymer enhanced oil recovery) technology in the petroleum industry: Prospects and challenges. *Energy* **77**, 963–982 (2014)
29. J. Villegas, I. Moncayo-Riascos, D. Galeano-Caro, M. Riazi, C.A. Franco, F.B. Cortés, Functionalization of γ-alumina and magnesia nanoparticles with a fluorocarbon surfactant to promote ultra gas-wet surfaces: Experimental and theoretical approach. *ACS Appl. Mater. Interfaces* (2020)

30. Y. Hurtado, C. Beltrán, R.D. Zabala, S.H. Lopera, C.A. Franco, N.N. Nassar, et al., Effects of surface acidity and polarity of SiO₂ nanoparticles on the foam stabilization applied to natural gas flooding in tight gas-condensate reservoirs. *Energy Fuel* **32**, 5824–5833 (2018)
31. S. Pérez-Robles, C.A. Matute, J.R. Lara, S.H. Lopera, F.B. Cortés, C.A. Franco, Effect of nanoparticles with different chemical nature on the stability and rheology of acrylamide sodium acrylate copolymer/chromium (III) acetate gel for conformance control operations. *Nano* **10**, 74 (2020)
32. H.S. Frank, W.-Y. Wen, Ion-solvent interaction. Structural aspects of ion-solvent interaction in aqueous solutions: A suggested picture of water structure. *Discuss. Faraday Soc.* **24**, 133–140 (1957)
33. Z. Amjad, Influence of iron oxide (rust) on the performance of phosphonates as calcium carbonate inhibitors, in *CORROSION 2016* (2016)
34. G. Graham, R. Stalker, R. McIntosh, The impact of dissolved iron on the performance of scale inhibitors under carbonate scaling conditions, in *International Symposium on Oilfield Chemistry* (2003)